Merging of Thin- and Thick-Film Fabrication Technologies: Toward Soft Stretchable "Island–Bridge" Devices

A. M. Vinu Mohan, NamHeon Kim, Yue Gu, Amay J. Bandodkar, Jung-Min You, Rajan Kumar, Jonas F. Kurniawan, Sheng Xu, and Joseph Wang**

Biointegrated soft electronic devices are expected to play crucial roles in consumer electronics,[1] healthcare,[2] and energy[3] domains to significantly transform our lifestyle. However, mating of conventional rigid electronic devices with soft biological tissues leads to significant compromise in performance.[4] The rapidly emerging field of soft, stretchable electronics has the potential to address this issue by ensuring conformal contact between wearable devices and the human body.[5] Researchers have mainly focused on using two approaches for realizing stretchable devices: deterministic[6] and random[7] composites. The deterministic composite route, also known as the "island–bridge" approach, involves lithographic fabrication of the device components onto rigid islands connected by serpentine bridges and ultimately bonding the device to a soft, stretchable elastomeric substrate.[8] When subjected to external strain, the underlying elastomeric substrate and the serpentine structures accommodate most of the stress, thus leaving the crucial device components unharmed.[5,9] On the other hand, random composite-based stretchability relies on the random incorporation of functional material within or on the elastomeric matrix to develop stretchable systems.[10]

Deterministically stretchable devices have an edge over their random composite counterparts since the performance of random composite devices diminishes by incorporating the functional components within/on elastomeric substrates.[11] In contrast, deterministic systems allow fabrication of complex, stretchable devices with performance similar to conventional rigid devices.[12] Additionally, lithographically fabricated deterministic stretchable systems can possess features with a few micrometer and even sub-micrometer dimensions, thus leading to compact, multifunctional devices. However, widespread applications of such devices are hindered since there are several materials that are incompatible with the lithographic fabrication route. For example, many devices rely on nanomaterials,[13] polymer composites,[14] carbonaceous,[15] biological,[16] low-temperature,[17] and solvent-sensitive[18] materials. Integrating these materials in microstructured forms on elastomeric substrates, for intimate contact with biological tissues, will open up new paradigms for wearable devices. High-precision scalable fabrication of such materials onto deterministically stretchable designs thus requires reliance on other fabrication techniques.

The key focus of the present work was to develop a strategy for combining lithography (thin-film) and screen-printing (thick-film) techniques to realize deterministic, high-performance stretchable devices. Screen printing has been widely used toward large-scale, cost-effective incorporation of a myriad of materials onto numerous substrates for various applications.[19,20] However, most of the printable inks form either rigid or flexible films. Developing stretch-enduring inks is challenging as only a handful of elastomeric binders and functional materials can be homogeneously dispersed to achieve high-performance stretchable inks. While lithographic and printing techniques have been the primary methods used for fabricating wearable devices, their distinct and complementary advantages and characteristics have not been combined.

The described new hybrid fabrication process, combining the printing of functional ink materials onto lithographically stretchable deterministic patterns, represents an attractive route that can address the challenges of each individual technique. For example, while lithography has been exploited for realizing complex stretchable systems, they are limited to thin films (<10 μm), which are not suitable for devices requiring high loading of active materials (e.g., energy harvesting and storage devices). In addition, there are limited choices of materials that can be vacuum deposited and solution etched. On the other hand, screen printing enables sufficient loading of a variety of active materials into thick (20–50 μm) films, but it suffers from meeting required layout resolutions and performance. In the hybrid system, the thick film resides over rigid isolated islands interconnected with free-standing stretchable serpentine bridges. The device can thus afford to include a wide range of rigid and lithographically incompatible materials without concern of device failure, since most of the strain is accommodated by the serpentine structures while leaving the thick-film islands unharmed. The hybrid system thus combines the best of two worlds.

The hybrid pattern has been realized by first lithographically fabricating the entire "island–bridge" layout of the device in gold onto an elastomeric substrate, followed by printing the ink layer on the islands (**Figure 1**A). Briefly, a polyimide-coated copper film was bonded to a polydimethylsiloxane-covered glass slide. Thereafter, copper electrodes were patterned via standard lithographic technique. Subsequently, gold electrodes were patterned onto the copper design. Later, a top layer of polyimide was patterned to define the active electrode area and finally transferred to an EcoFlex layer. Subsequently, the device was transferred to the printer where electrodes were screen printed with inks. The detailed fabrication process is described in the

Dr. A. M. V. Mohan, N. Kim, Y. Gu, Dr. A. J. Bandodkar, Dr. J.-M. You, R. Kumar, J. F. Kurniawan, Prof. S. Xu, Prof. J. Wang
Department of NanoEngineering
University of California
San Diego, La Jolla, CA 92093, USA
E-mail: shengxu@ucsd.edu; josephwang@eng.ucsd.edu

DOI: 10.1002/admt.201600284

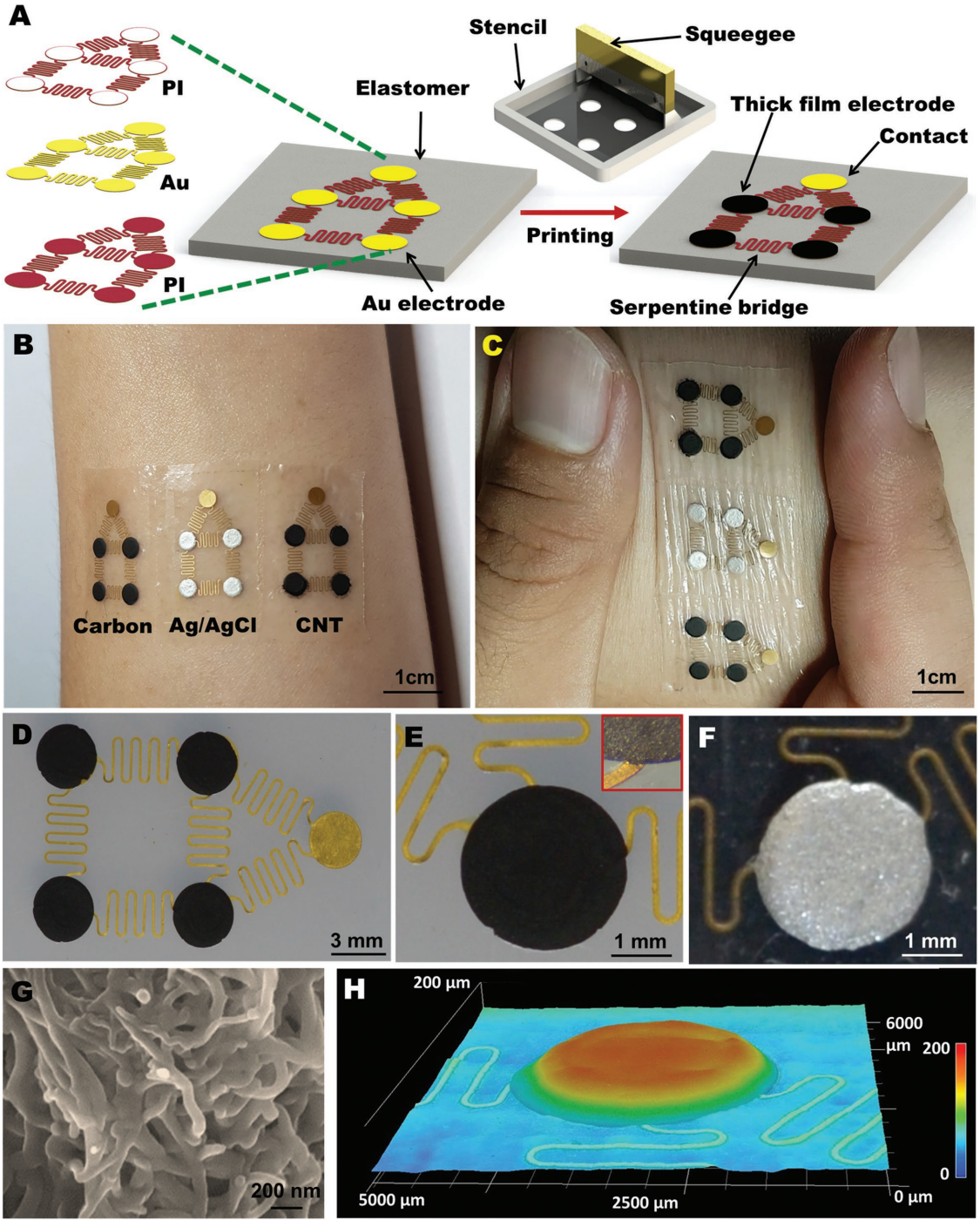

Figure 1. Soft stretchable devices prepared by merging thin- and thick-film fabrication technologies. A) Scheme showing fabrication of the hybrid thick–thin stretchable electrode system, including the lithographic and printing steps (left and center, respectively). B) Image showing an array of carbon (left), Ag/AgCl (center), and CNT (right) based electrodes applied to the forearm of a human subject. C) Image of the skin-mounted device when pinched. Optical microscopic image of the D) entire system and close-up showing the registration of the E) carbon (inset demonstrates close-up image of the thick–thin-film interface), and F) Ag/AgCl ink onto the underlying Au electrode. G) SEM of the CNT film printed onto the Au electrode. H) 3D optical image clearly depicting the thick–thin feature of the hybrid electrode system.

Supporting information. The circular island electrodes can then be patterned with a wide range of printable inks. The soft, stretchable nature of such hybrid devices allows intimate and easy integration with the human epidermis (Figure 1B) while maintaining structural integrity and minimizing delamination from the skin when subjected to multiaxial strains (Figure 1C; Video S1, Supporting Information). The versatility of such a hybrid fabrication process has been demonstrated by printing

various carbon, Ag/AgCl, enzyme-loaded Prussian Blue, and carbon nanotube (CNT)-based inks due to their widespread use in energy, sensing and electrochromic-display applications (Figure 1B–F). For example, the dramatically enhanced sensing performance of the new hybrid carbon–gold thick–thin electrode system compared to its bare gold thin-film counterpart has been demonstrated for the detection of important analytes, including nitroaromatic explosives, catecholamine neurotransmitters, glucose, and nucleic acids, as well as epidermal biosensing of sweat lactate.

The hybrid electrode system has been designed to endure mechanical strains caused by bodily movements. Keeping cognizance of such a requirement, it was designed in the form of a square, with the electrodes present at its corners as circular islands with freestanding serpentine interconnects, bridging the adjacent electrode islands (Figure 1D). While the new island–bridge hybrid concept is illustrated here using four adjacent electrodes toward wearable sensors, it could be readily scaled up to cover larger areas of the skin to meet the demands of specific applications (e.g., epidermal biofuel cells). The orthogonally located free-standing serpentine interconnects impart stretchability to the device in all directions along its plane, thus enabling it to withstand repeated uniaxial and biaxial strains common to the human epidermis. Thin- and thick-film microfabrication techniques were seamlessly combined to achieve uniform registration of printable inks onto the gold backbone, as clearly depicted in Figure 1E,F. These images illustrate the perfect overlap of the printed films onto the gold islands with minimal line edge roughness. Figure 1G showcases a scanning electron microscope (SEM) image focusing on the uniform printability and distribution of the CNT ink printed on top of a gold island. Apart from the homogeneous printability, the printed films must also adhere strongly to the gold surface under repeated multiaxial stretching deformations. Figure 1H illustrates the huge difference in thickness of Au and printed films. In general, the strain is proportional to film thickness. Hence, the stretchability of thin gold films is much larger than that of the thick printed layers. However, the mismatch between the thicknesses of the two films is not a major issue for the present system due to its island–bridge design. As illustrated in Figure 1C, and Figure S1 and Video S1 in the Supporting Information, the skin-worn hybrid system is able to defiantly withstand repeated pinching (50 times) with virtually no impact on its structural integrity. Such impressive stretchability reflects the system's strategic design that leads to most of the applied strain to be accommodated by the serpentine structures while rendering the thick printed electrode unaffected.

Strain can have deleterious impact on conductivity of the system. Potential sources of such resistance variations include (1) piezoresistance of the copper and/or gold interconnects and (2) interfacial delamination between the thin-metal island and the overlaid printed thick films. In the first set of experiments, a hybrid device (**Figure 2**A) was connected to a multimeter and linearly stretched in increments of $\varepsilon = 25\%$ till the strain reached $\varepsilon = 75\%$ (Figure 2B), followed by decreasing strain until it reached its initial state ($\varepsilon = 0\%$; Figure 2C). As illustrated in Figure 2D, the resistance of the hybrid (C–Au) electrode system varies negligibly, with a relative standard deviation (RSD) of 1.75%, in a manner similar to that of the thin gold electrodes (RSD = 1.26%). It is important to point out that the hybrid C–Au structure is orders of magnitude thicker than the pristine gold electrode, as clearly illustrated by the 3D optical image in Figure 1H; yet, its stretchability is similar to that of the thin gold electrode because of the island–bridge design. The slightly higher resistance of the C–Au hybrid system than the pristine metal structure reflects the higher resistivity of the printed carbon layer as compared to the bare gold electrode. The variation in the resistance of the hybrid system under biaxial strain was also studied (Figure 2E–H). The strain was increased from 0% (Figure 2E) to 75% (Figure 2F) with a step of $\varepsilon = 25\%$ and finally brought back to its initial state (Figure 2G). Similar to the uniaxial stretching experiments, the bare thin gold electrode system and the C–Au hybrid system showed negligible variation in resistance as a function of repeated biaxial stretching with RSD = 1.93% and 0.69%, respectively (Figure 2H). Close-up visual inspection of the system during these repeated physical deformations revealed no apparent delamination of the printed layer, reflecting the strong adhesion of the printed island electrodes to the gold surface.

The elasticity of the hybrid stretchable device was analyzed by comparing its Young's modulus (8.63 psi) with that of a control Ecoflex substrate (7.1 psi). As shown in Figure S2 (Supporting Information), the hybrid device leads to a very small change in elasticity versus the control substrate. Such small variation reflects that the hybrid system behaves just like an elastomeric material even when it consists of tens of micrometers thick rigid carbon film on the gold islands. Thus, rigid layers of various materials can be incorporated within the hybrid system while still maintaining its soft, stretchable nature similar to that of elastomers.

The effect of stretching on the electrochemical response of the hybrid system was analyzed by recording cyclic voltammograms (CVs) after repeated uniaxial stretching of the electrode system at $\varepsilon = 75\%$. Ferricyanide (a common redox probe) and dopamine (an important neurotransmitter) were selected as candidates to assess potential variations in electrochemical response. The minimal impact on the voltammetric response during these tests for both ferricyanide (Figure 2I) and dopamine (Figure 2J) highlights the resilience of the system toward such strains. Moreover, the electron transfer kinetics occurring at the electrode–electrolyte interface was also studied (Figure S3, Supporting Information). The gradual separation of peak and linear relation between peak current height and square root of scan rate implies that the electron transfer follows a quasireversible route, as reported for several printed carbon electrodes.[21] The effect of biaxial stretching on the electrochemical response of the system toward ferricyanide and dopamine was also examined. Figure 2K,L illustrates that repeated biaxial stresses had a negligible impact on the voltammetric response with the recorded CVs remaining virtually identical.

The primary focus of the present work was to demonstrate the development of stretchable devices that could be realized by the synergistic effect of combining the attributes of lithography and printing. Carbonaceous materials have long been the preferred electrode material over noble metals, such as gold, due to their low background current, high overvoltage for electrolysis of water and hydrogen evolution, and hence a wide potential window, and attractive electrochemical reaction

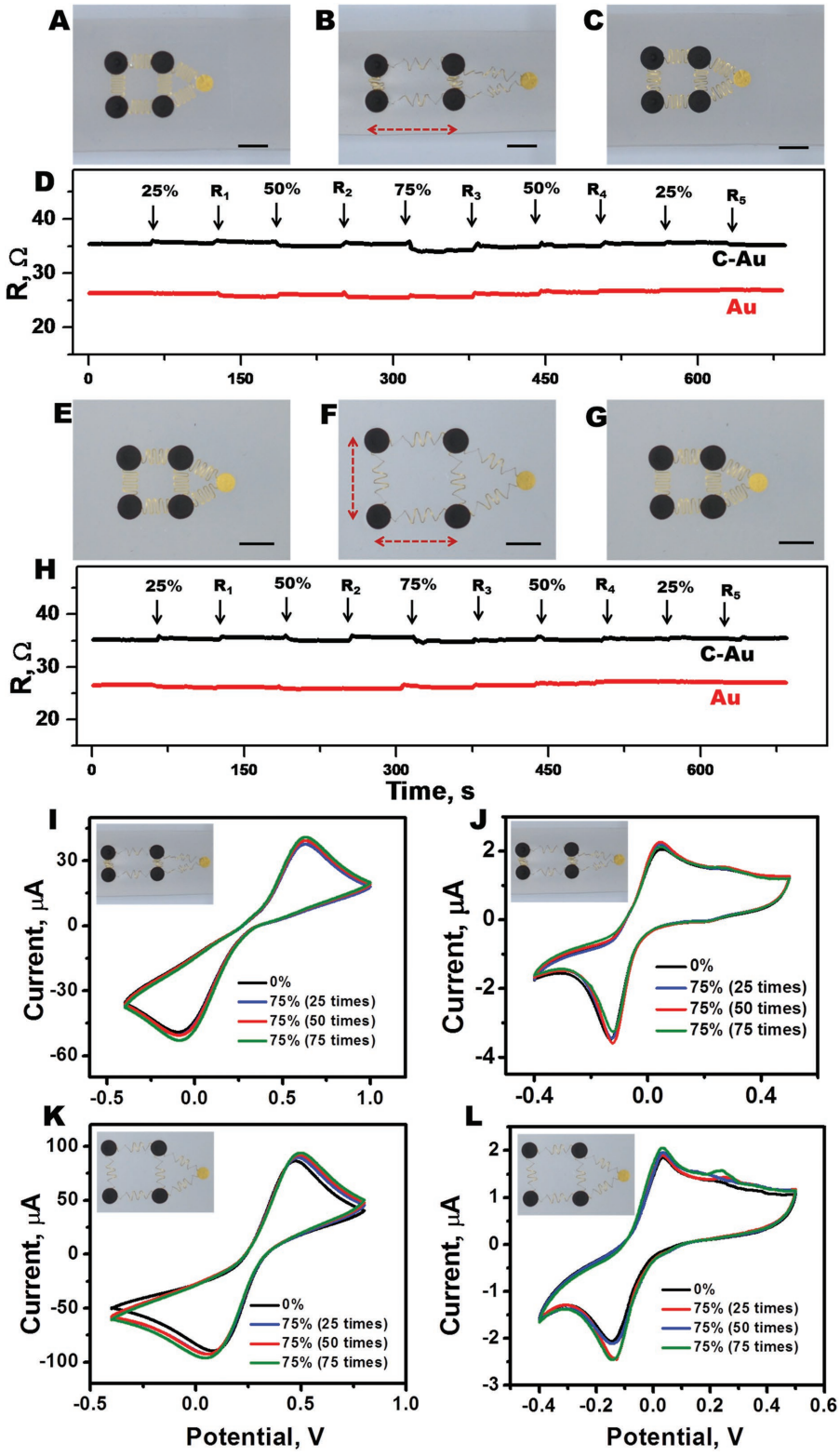

Figure 2. Endurance toward repeated stretching. Images showing the electrode system A) before, B) during (arrow showing the direction of stretching), and C) after linear stretching ($\varepsilon = 75\%$). D) Real-time evolution of resistance as a function of linear stretching for bare Au and C–Au electrode systems (R1–R5 indicate releasing the tensile load). Images showing the electrode system E) before, F) during (arrow showing the direction of stretching), and G) after biaxial stretching ($\varepsilon = 75\%$). H) Real-time evolution of resistance as a function of biaxial stretching for bare Au and carbon on the Au electrode system. CVs recorded for the C–Au electrode system after repeated uniaxial stretching ($\varepsilon = 75\%$) for I) 10×10^{-3} M ferricyanide and J) 100×10^{-3} M dopamine. CVs recorded for the C–Au electrode system after repeated biaxial stretching ($\varepsilon = 75\%$) for K) ferricyanide and L) dopamine. A–C,E–G) Scale bar: 5 mm. Scan rate: 0.1 V s^{-1}.

kinetics.[22] Incorporation of carbonaceous materials with the lithographically designed stretchable devices can have major implications in energy[23] and sensing[24] sectors.

The advantages of the new carbonaceous stretchable devices were demonstrated for electrochemical sensing of important analytes, including nitroaromatic explosives, catecholamine neurotransmitters, and nucleic acids (**Figure 3**A–D). Figure 3A compares square-wave voltammograms (SWV) for the explosive 2,4-Dinitrotoluene (DNT) at the hybrid C–Au thick–thin electrode system and its bare gold counterpart. Electrochemical detection of DNT usually involves identifying the reduction peaks of its two nitro groups.[25,26] Unfortunately, the reduction occurs at quite negative potentials. Hence, it is imperative to select electrode materials, such as carbon, which has high overvoltage for hydrogen evolution as compared to noble materials, like gold, wherein high background current is obtained to do electrolysis of water. Figure 3A illustrates that the C–Au system offers favorable well-defined and separated reduction peaks of the two nitro groups of DNT along with a low background current over the entire potential range. In contrast, the gold system displays a single broad reduction peak and high background current starting from –0.7 V (that obscures the second peak). The C–Au system was thus utilized to detect various trace concentrations of DNT in aqueous media (Figure 3B), offering a well-defined response, proportional to the explosive concentration, and favorable signal-to-background characteristics. The merit of printing carbon electrodes on the gold islands was further demonstrated toward the detection of single-stranded DNA using the bare gold and C–Au systems (Figure 3C). It is well documented that carbon electrodes offer the most favorable anodic detection of nucleic acids based on

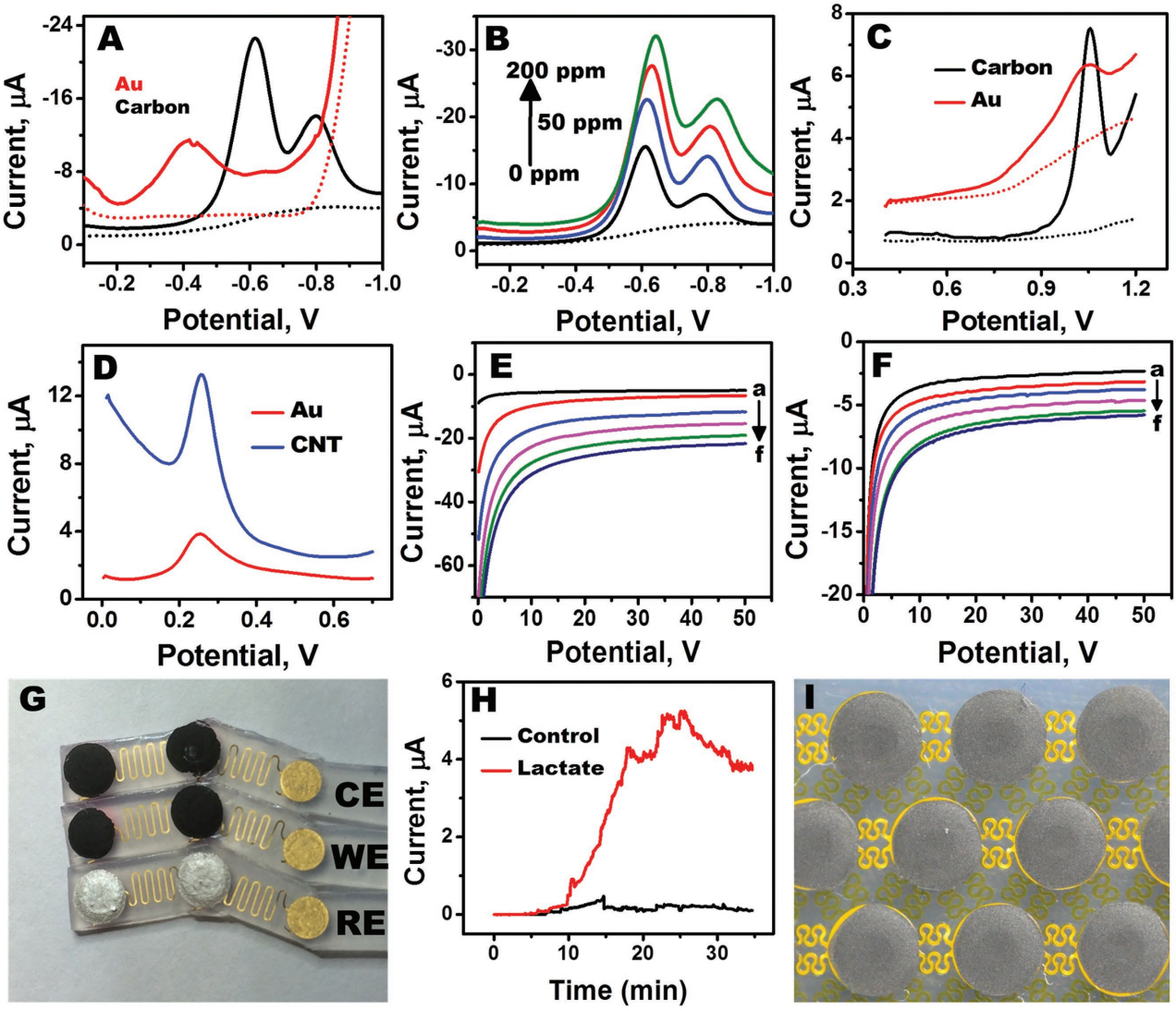

Figure 3. A) Reductive SWVs recorded for Au (red) and carbon (black) electrode systems for 100 ppm DNT (thick lines) and 0 ppm DNT (dotted lines). B) Reductive SWVs recorded for the Au electrode system for 0–200 ppm DNT. C) SWVs recorded for carbon (black) and Au (red) electrodes for 25 µg mL^{-1} (thick lines) and 0 µg mL^{-1} (dotted lines) ssDNA in 0.1 M acetate buffer (pH 4.65). D) SWVs recorded for Au (red) and CNT (blue) electrode systems for 100×10^{-6} M dopamine. E) Chronoamperograms recorded for the Prussian Blue–carbon–GOx electrode system for 0–25×10^{-3} M glucose at an applied potential of –0.2 V. F) Chronoamperograms recorded for Prussian Blue–carbon–LOx electrode system for 0–15×10^{-3} M lactate at an applied potential of –0.2 V. G) An image showing the stretchable lactate sensor having working, reference, and counter electrodes. H) Real-time on-body amperometric evaluation of lactate levels of a subject with (red) and without (black) enzyme modification. I) An optical image that demonstrates the feasibility of large-scale patterning of stretchable thick–thin-film islands for various energy applications.

direct oxidation of guanine.[27] Figure 3C highlights the superior DNA detection ability of C–Au electrode as compared to Au involving sharp peak, low background current, and wide anodic potential window.

CNT-based electrode materials have several advantages in energy and sensing fields.[28] However, integration of CNTs into stretchable lithographic systems is cumbersome and expensive. Screen printing has been used for fabricating CNT-based devices.[29] In the present work, customized CNT ink,[30] was utilized to realize CNT films onto the stretchable gold electrode system. The advantage of the CNT–Au system over its bare gold counterpart is even more pronounced toward measurements of the important neurotransmitter dopamine (Figure 3D). The CNT–Au electrode displays a significantly sharper and larger SWV oxidation peak compared to the bare gold electrode. The CNT–Au electrode also displayed enhanced electron-transfer characteristics toward ferrocyanide, as compared to C–Au and bare gold electrodes (Figure S4, Supporting Information).

Integrating biotic and abiotic components to develop bio-integrated systems is quite essential for various healthcare applications.[31] However, most biological materials are quite labile to surrounding environment and lose their properties under harsh conditions encountered during lithographic processes. Thus, direct incorporation of biomaterials with lithography is daunting. Combining printing with lithography can provide an attractive route to functionalize lithographically

patterned devices with a wide range of biotic components. Enzymatic glucose and lactate electrochemical biosensors were evaluated to demonstrate the viability of the new thick–thin hybrid fabrication process toward realizing soft bioelectronic systems. Glucose oxidase and lactate oxidase enzymes were homogeneously dispersed within Prussian Blue ink and then subsequently printed onto the gold island electrodes. Prussian Blue ink was selected due to its high selectivity toward the hydrogen peroxide product of the enzymatic reactions.[32] The data for glucose (Figure 3E) and lactate (Figure 3F) illustrate the linear response of these enzymatic electrodes toward their respective analytes. The ease with which such labile biocatalytic moieties could be successfully incorporated onto the stretchable platform emphasizes again the importance of the hybrid thick–thin fabrication process. Similar printing protocol can be employed to include other biological components for various bioelectronic applications.

The stretchable hybrid lactate biosensor was evaluated for real-time epidermal monitoring of sweat lactate.[33] The dynamic concentration changes of lactate in human perspiration were measured continuously during a 33 min intense cycling activity following a profile illustrated in Figure S5 (Supporting Information). The stretchable lactate sensor (Figure 3G) was placed on the subject's deltoid and interfaced with a handheld electrochemical analyzer. Figure 3H reveals the continuous amperometric data recorded for both lactate sensor (red) and enzyme-free control (black) stretchable electrodes during the cycling activity. In the presence of enzyme, the sensor exhibits facile biocatalytic efficiency toward the oxidation of lactate in the sweat. No apparent current response is observed at the initial stages of the cycling at both the electrodes, reflecting the absence of sweat. The epidermal sensor starts to measure the current response, proportional to the lactate level, as the subject begins to perspire at ≈900 s. The sweat lactate level increases upon increasing the cycling intensity, as indicated from the rising current signal. A decreased current signal is observed after 24 min, reflecting the decreased lactate sweat level associated with the slower exercise intensity and sweat dilution (Figure S5, Supporting Information). As expected, no current response is observed using the control transducer (without the enzyme).

The hybrid "island–bridge" approach also provides the feasibility of scalable patterning of larger stretchable devices based on the requirements for diverse energy generation and storage applications. Figure 3I demonstrates such a hybrid array device, patterned on the stretchable substrate that could be used as a wearable energy-harvesting device.

We reported on the amalgamation of thick- and thin-film fabrication techniques for preparing high-performance stretchable "island–bridge" devices with different functional materials. Screen printing has been used to prepare the rigid printed (island) electrodes while thin-film lithography employed for fabricating the serpentine interconnects (bridges). The resulting hybrid stretchable systems display new capabilities that cannot be achieved through the individual fabrication routes. The new hybrid fabrication strategy can lead to a variety of deterministic stretchable structures with a broad range of functional materials, based on the judicious choice of the ink material and modifier. For example, the printing of various carbons or enzymes has led to a powerful platform for sensitive and selective electrochemical sensing of explosives, neurotransmitter, nucleic acids, glucose, and lactate, without affecting its stretchability. However, the present hybrid approach has certain limitations. For example, the printing technique cannot fabricate few micrometer/sub-micrometer features that can be reliably developed by lithographic techniques, thus impeding the use of the hybrid fabrication process for realizing systems with few micrometer/sub- micrometer features. This can be addressed partially by using tailored-made inks and stencils that lead to significant improvement in the printing resolution with features down to a few tens of micrometer widths.[34] Inefficient bonding of the printed layer to the lithographically fabricated metal film is another possible issue as it can lead to delamination of the printed film when the device is subjected to extreme tensile load. This can be mitigated by surface engineering the metal film via added ink modifiers that enhance the bonding of the printed film to the metal surface. Although there are some limitations, these issues can be addressed to exploit the distinct advantages of the new thin-film/thick-film deterministic approach for a wide range of flexible and wearable electronic applications.

Experimental Section

The evaluation of the epidermal biosensor was performed in strict compliance with a protocol approved by the institutional review board (IRB) at the University of California, San Diego.

Supporting Information

Supporting Information is available from the Wiley Online Library or from the author.

Acknowledgements

A.M.V.M., N.K., Y.G., and A.J. contributed equally to this work. This work was supported by DTRA (HDTRA1-16-1-0013), NIH (Award No. R21EB019698), and DOE ARPA-E (DE-AR0000535). R.K. acknowledges the National Science Foundation Graduate Research Fellowship under Grant No. DGE-1144086.

Received: December 7, 2016
Revised: December 22, 2016
Published online: February 15, 2017

[1] J. Ouyang, C. Chu, C. R. Szmanda, L. Ma, Y. Yang, *Nat. Mater.* **2004**, *3*, 918.
[2] C. H. Lee, H. Kim, D. V. Harburg, G. Park, Y. Ma, T. Pan, J. S. Kim, N. Y. Lee, B. H. Kim, K. Jang, S. Kang, Y. Huang, J. Kim, K. Lee, C. Leal, J. A. Rogers. *NPG Asia Mater.* **2015**, *7*, 227.
[3] M. Koo, K. Park, S. H. Lee, M. Suh, D. Y. Jeon, J. W. Choi, K. Kang, K. J. Lee, *Nano Lett.* **2012**, *12*, 4810.
[4] D. Kim, R. Ghaffari, N. Lu, J. A. Rogers, *Annu. Rev. Biomed. Eng.* **2012**, *14*, 113.
[5] D. H. Kim, N. Lu, R. Ma, Y. S. Kim, R. H. Kim, S. Wang, J. Wu, S. M. Won, H. Tao, A. Islam, K. J. Yu, T. Kim, R. Chowdhury, M. Ying, L. Xu, M. Li, H. J. Chung, H. Keum, M. McCormick, P. Liu,

Y. W. Zhang, F. G. Omenetto, Y. Huang, T. Coleman, J. A. Rogers, *Science* **2011**, *333*, 838.
[6] D. S. Grey, J. Tien, C. S Chen, *Adv. Mater.* **2004**, *16*, 393.
[7] J. A. Fan, W. Yeo, Y. Su, Y. Hattori, W. Lee, S. Jung, Y. Zhang, Z. Liu, H. Cheng, L. Falgout, M. Bajema, T. Coleman, D. Gregoire, R. J. Larsen, Y. Huang, J. A. Rogers, *Nat. Commun.* **2014**, *5*, 3266.
[8] M. Melzer, G. Lin, D. Makarov, O. G. Schmidt, *Adv. Mater.* **2012**, *24*, 6468.
[9] Y. Zhang, S. Xu, H. Fu, J. Lee, J. Su, K. Hwang, J. A. Rogers, Y. Huang, *Soft Matter* **2013**, *9*, 8062.
[10] M. Park, J. Im, M. Shin, Y. Min, J. Park, H. Cho, S. Park, M. Shim, S. Jeon, D. Chung, J. Bae, J. Park, U. Jeong, K. Kim, *Nat. Nanotechnol.* **2012**, *7*, 803.
[11] D. J. Lipomi, *Adv. Mater.* **2016**, *28*, 4180.
[12] J. A. Rogers, T. Someya, Y. Huang, *Science* **2010**, *327*, 1603.
[13] P. Lee, J. Lee, H. Lee, J. Yeo, S. Hong, K. H. Nam, D. Lee, S. S. Lee, S. H. Ko, *Adv. Mater.* **2012**, *24*, 3326.
[14] Z. Yu, X. Niu, Z. Liu, Q. Pei, *Adv. Mater.* **2011**, *23*, 3989.
[15] Y. Zhang, Q. Chen, J. Ge, Z. Liu, *Chem. Commun.* **2013**, *49*, 9815.
[16] L. Xiao, Z. Chen, C. Feng, L. Liu, Z. Bai, Y. Wang, L. Qian, Y. Zhang, Q. Li, K. Jiang, S. Fan, *Nano Lett.* **2008**, *8*, 4539.
[17] S. H. Ko, H. Pan, C. P. Grigoropoulos, C. K Luscombe, J. M. J. Frechet, D. Poulikakos, *Nanotechnology* **2007**, *18*, 345202.
[18] T. Sekitani, T. Someya, *Adv. Mater.* **2010**, *22*, 2228.
[19] M. Li, Y. Li, D. Li, Y. Long, *Anal. Chim. Acta* **2012**, *734*, 31.
[20] A. J. Bandodkar, I. Jeerapan, J. Wang, *ACS Sens.* **2016**, *1*, 464.
[21] H. Wei, J. Sun, Y. Xie, C. Lin, Y. Wang, W. Yin, G. Chen, *Anal. Chim. Acta* **2007**, *588*, 297.
[22] R. L. McCreery, *Chem. Rev.* **2008**, *108*, 2646.
[23] S. Xu, Y. Zhang, J. Cho, J. Lee, X. Huang, L. Jia, J. A. Fan, Y. Su, J. Su, H. Zhang, H. Cheng, B. Lu, C. Yu, C. Chuang, T. Kim, T. Song, K. Shigeta, S. Kang, C. Dagdeviren, I. Petrov, P. V. Braun, Y. Huang, U. Paik, J. A. Rogers, *Nat. Commun.* **2013**, *4*, 1543.
[24] X. Wang, T. Li, J. Adams, J. Yang, *J. Mater. Chem. A* **2013**, *1*, 3580.
[25] Y. T. Yew, A. Ambrosi, M. Pumera, *Sci. Rep.* **2016**, *6*, 33276.
[26] J. Wang, *Electroanalysis* **2007**, *19*, 415.
[27] J. Wang, X. Cai, J. Wang, C. Jonsson, E. Palecek, *Anal. Chem.* **1995**, *67*, 4065.
[28] M. F. L. De Volder, S. H. Tawfick, R. H. Baughman, A. J. Hart, *Science* **2013**, *339*, 535.
[29] J. Wang, M. Musameh, *Analyst* **2004**, *129*, 1.
[30] A. J. Bandodkar, I. Jeerapan, J. You, R. Nunez-Flores, J. Wang, *Nano Lett.* **2016**, *16*, 721.
[31] D. Kim, J. Viventi, J. J. Amsden, J. Xiao, L. Vigeland, Y. Kim, J. A. Blanco, B. Panilaitis, E. S. Frechette, D. Contreras, D. L. Kaplan, F. G. Omenetto, Y. Huang, K. Hwang, M. R. Zakin, B. Litt, J. A. Rogers, *Nat. Mater.* **2010**, *9*, 511.
[32] A. A. Karyakin, *Electroanalysis* **2001**, *13*, 813.
[33] A. J. Bandodkar, W. Jia, C. Yardımcı, X. Wang, J. Ramirez, J. Wang, *Anal. Chem.* **2015**, *87*, 394.
[34] Y. J. Hyun, S. Lim, B. Y. Ahn, J. A. Lewis, C. D. Frisbie, L. F. Francis, *ACS Appl. Mater. Interfaces* **2015**, *7*, 12619.